AIAA Journ. of Guidance, Control, and Dynamics, Vol. 21, No. 2, 1998, pp. 264-270.

Nonlinear Input Shaping Control of Flexible Spacecraft Reorientation Maneuver*

Dimitry Gorinevsky† and George Vukovich‡

Abstract

This paper presents a design of a novel feedforward controller for a large-angle reorientation maneuver of a spacecraft with flexible appendages, such as a telecommunication satellite. The controller combines collocated feedback and feedforward control. It uses an efficient and conceptually simple numerical method for the computation for an optimal feedforward input shape for a nonlinear flexible system. The method is based on a minimization of a single regularized performance index instead of solution of a terminal control problem. The paper describes a proposed flexible spacecraft testbed developed at the Canadian Space Agency, and studies application of the designed control scheme to this testbed. The designed controller is shown to provide excellent performance in compensation of residual flexible vibrations for the nonlinear system in question.

*This work was supported by the Canadian Space Agency contract # 9F028-4-3515/01-XSD

†Adjunct Professor, Department of Electrical and Computer Engineering, University of British Columbia, 2356 Main Mall, Vancouver, B.C., Canada V6T 1W5, email: gorin@ee.ubc.ca

‡Directorate of Space Mechanics, Canadian Space Agency, 6767 Route de L'Aeroport, St.-Hubert, Quebec, Canada J3Y 8Y9

1 Introduction

Many second-generation and proposed third-generation spacecraft have or are likely to have very flexible appendages, such as solar arrays and antennae. It is generally necessary to control reorientation of such spacecraft so that little flexible vibration of appendages is excited. Because of the substantial flexibility, the period of the main oscillation mode(s) can be comparable to reorientation maneuver duration. Thus, nonlinear rotational dynamics of the spacecraft can interact with the flexible dynamics, making vibration control a difficult nonlinear problem.

A practical means of controlling a nonlinear flexible system is to use a combination of feedback and feedforward control. Measurement of flexible appendage deformation is not collocated with attitude actuation (thruster jets or flywheels), and because of this, the achievable performance of the feedback is limited. Proper design of a feedforward control can do much to alleviate this problem.

This paper describes a testbed for large-angle attitude maneuver control of a flexible spacecraft. It develops and applies a novel feedforward control technique, which is related to a number of approaches collectively known as "input shaping control." The nonlinear controller designed in this paper is based on off-line iterative optimization of a feedforward control shape. The proposed feedforward control design method is very simple conceptually and requires to have only a forward simulation model of the system.

The goal of this input shaping control is to avoid excitation of residual vibrations at the end of the maneuver. We consider some prior work in this area.

A number of approaches developed for *linear* flexible systems shape a feedforward input so that it does not contain spectral components at system eigenfrequencies. Early papers on input shaping consider feedforward defined by a finite expansion, e.g., trigonometric [1, 2, 3, 4, 5, 6]. A version of the same approach using a pulse sequence expansion was proposed by Singer and Seering [7]. They, and a number of other researchers (e.g., see [8, 9, 10]) made use of the fact that a spectrum of a *convolution* of two signals is the product of two signal spectra, which produces a zero excitation at frequencies where one or the other of the spectra is zero. A convolution of a command signal with a pulse sequence is a weighted sum of time-delayed copies of the signal and can be conveniently implemented once the pulse sequence is known. The computation of the proper pulse sequence can be considered as the design of a notch filter to remove the resonance excitation from the command signal.

The approach developed by Bayo and coworkers [11, 12] uses a frequency-based inverse dynamics technique for computation of a noncausal feedforward transfer function for tracking a desired acceleration profile with a flexible system end-point. An experimental application of this approach to flexible link control is considered in [12]. The technique is very demanding computationally.

The general problem with the frequency-based input shaping methods discussed above is that they are for linear systems. Modifications of such methods for nonlinear flexible systems are usually based on small nonlinearity and robustness assumptions and can yield significant levels of residual vibration when these assumptions do not hold [12, 13, 14]. Input shaping techniques based on time-domain representations and optimization of control inputs are usually easier to generalize for nonlinear flexible system control than are the frequency-domain approaches. Such time-domain approaches are mostly based on one of the two following ideas. The first is to use some kind of inverse dynamics computation given the planned end-point trajectory. The second is to apply some type of optimization technique to find an entire feedforward function which allows satisfaction of the terminal conditions.

A practical approach to the control of flexible systems which was developed and successfully applied in experiments in [15, 16, 17] is to combine a feedback with a feedforward of rigid-body dynamics and a quasistatic flexible deflection. With this approach, the feedforward compensation of flexible dynamics is not exact, and is only successful if the feedback performance is good. Another practical example of combining feedback and feedforward in control of flexible structure can be found in [18].

Some time-domain approaches compute the feedforward control within a given interval as an expansion of some shape functions. The expansion weights are computed to minimize a quadratic performance index which can represent trajectory tracking quality [19, 20, 21], or a weighted sum of trajectory tracking and terminal error penalties [22]. The performance index also might include a quadratic penalty for control resources that corresponds to fuel-optimal control of a flexible spacecraft [23] or a combination of time, fuel, and robustness constraints [24]. These approaches give excellent practical results, but if directly applied to a terminal control problem might require involved iterative algorithms to solve a boundary-value optimization problem.

In this paper, we demonstrate a feedforward shaping controller based on an efficient numerical optimization procedure. Instead of solving the boundary-value problem, a single quadratic performance index is minimized. The index includes a terminal penalty and results in a very small terminal error as demonstrated in the simulation example. By combining the feedforward with collocated feedback controller, we demonstrate efficient control of large-angle slewing maneuvers for a flexible spacecraft testbed. This paper considers reorientation maneuvers for a spacecraft with two symmetrical flexible appendages.

2 Testbed for spatial slewing control of flexible spacecraft

This section presents a dynamical model and simulation results for a laboratory testbed of a flexible slewing system. This testbed is currently under development in the Directorate of Space Mechanics of the Canadian Space Agency.

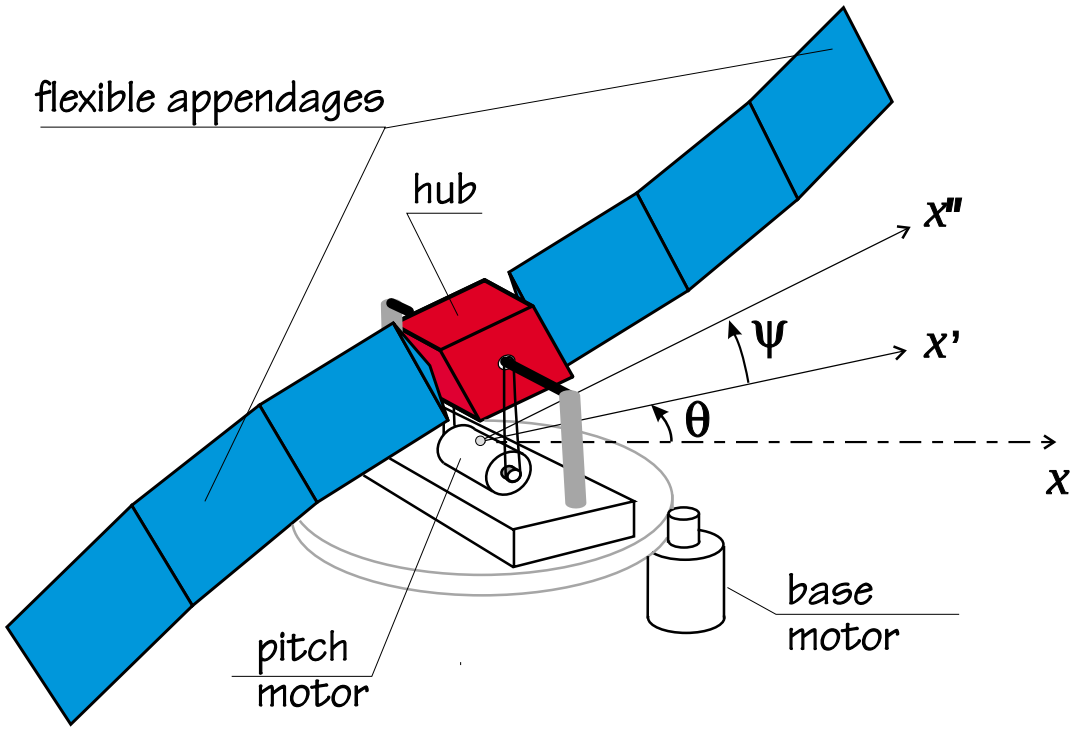

Figure 1: Proposed CSA flexible spacecraft setup for control of large-angle slewing

A number of setups exist which allow for spatial rotation of flexible systems. Examples are DAISY in University of Toronto Institute of Aerospace Studies (UTIAS) in Canada and ASTREX facility in Phillips Laboratory at Edwards Air Base in USA. These setups are very expensive devices that are difficult to maintain and operate. They use air bearings for the support of the central body. Unlike these, the CSA flexible satellite testbed is a relatively simple setup using inexpensive DC motor technology and a straightforward mechanical design. At the same time, it exhibits features typical of nonlinear flexible dynamics of spatial slewing maneuvers and is thus appropriate for the development of suitable control technology.

The setup is schematically shown in Figure 1. The main part of the setup is a rigid hub with two flexible appendages. The system represents a configuration with some similarities to a typical telecommunication satellite with appendages modeling solar arrays.

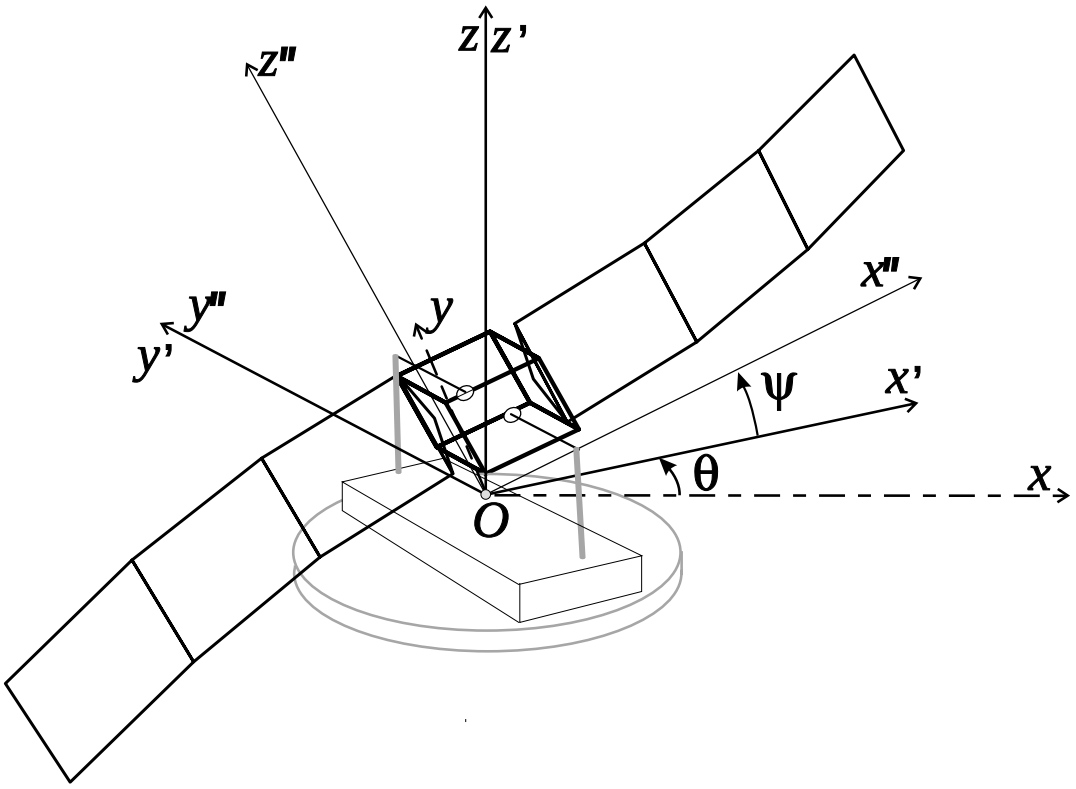

Figure 2: Coordinate frames for the CSA flexible spacecraft setup

The hub is suspended to allow for rotation with respect to the horizontal axis perpendicular to the beam axis. This rotation (pitch angle ψ) is controlled by an electric motor. The entire setup including the pitch motor is mounted on a fixed base. A second motor rotates the base with respect to the vertical axis passing through the base center (yaw angle θ). A third motor could be added to the setup, providing for roll motion of the hub with beams, thus making possible an arbitrary controlled spatial rotation of the system.

2.1 Dynamics of the system

The coordinate frames attached to the CSA flexible spacecraft setup are shown in Figure 2. The inertial coordinate frame $Oxyz$ has a vertical axis Oz passing through the base and hub centers. The coordinate frame $Ox'y'z'$ is attached to the base and is obtained from $Oxyz$ by rotation on the angle θ around the axis Oz. The frame $Ox''y''z''$ is attached to the hub and is obtained from $Ox'y'z$ by rotation on the angle ψ around the axis Oy'. The axis Ox'' of the last coordinate frame is parallel to the appendages in the undeformed state.

Let us denote by J the moment of inertia of the rotating base together with the rotor of the base drive and all bodies fixed to the base. The moment of inertia J includes pitch drive and excludes the hub with the appendages. Let us denote by I_2 the joint moment of inertia of the hub with respect to the axis Oy'' and the rotor of the pitch motor. It is assumed that the center of mass of the hub is on the intersection of the base and pitch rotation axes and that moments of inertia of the hub with respect to the axes Ox'' and Oz'' are equal to I_1.

Our model of flexible dynamics of the appendages is based on the following assumptions:

- The appendages are identical and attached (clamped) symmetrically with respect to the hub center. They

can be considered as uniform beams and their bending deformations in the plane $Ox''z''$ can be described using the Euler-Bernoulli model.

- Stiffness of the appendages in the vertical plane is very high and their deformation in this plane can be neglected.
- Frequencies of torsional modes of the beam vibration are much higher than that of the first few bending modes, so that torsional vibrations can be neglected.
- Only the first few bending modes of vibration need to be taken into account to get a practically satisfactory description of the system flexible dynamics.

The appendages have linear density (mass per unit length) μ, length L each, and are attached at a distance a from the hub center. Bending stiffness of the appendages in the plane $Ox''y''$ is EI. We denote by $y(t,\xi)$ the flexible deflection for each of the two appendages along the axis Oy'', where t is time and ξ is a coordinate along the axis Ox''.

The kinetic energy of the system is composed of kinetic energies of the base, the hub, and the two appendages. This kinetic energy can be written in the form

$$T = \frac{1}{2}(J + I_1)\dot{\theta}^2 + \frac{1}{2}(I_2 + J_a)\dot{\psi}^2 + \frac{1}{2}\mu\int_{-(L+a)}^{-a}(\xi\cos\psi\dot{\theta} + \dot{y})^2 d\xi + \frac{1}{2}\mu\int_{a}^{L+a}(\xi\cos\psi\dot{\theta} + \dot{y})^2 d\xi, \tag{1}$$

where the dot denotes differentiation with respect to time. In (1), J_a is the moment of inertia of two appendages considered as rigid bodies, $J_a = 2\mu[(L+a)^3 - a^3]/3$.

As the system is symmetrical with respect to the pitch axis, the potential energy does not include a gravity term and is just the usual potential energy of beam bending deformation of the form

$$\Pi = \frac{1}{2}EI\int_{-(L+a)}^{-a}\left(\frac{\partial^2 y(t,\xi)}{\partial\xi^2}\right)^2 d\xi + \frac{1}{2}EI\int_{a}^{L+a}\left(\frac{\partial^2 y(t,\xi)}{\partial\xi^2}\right)^2 d\xi, \tag{2}$$

To derive the dynamical model of the described system, we will use the Galerkin (assumed modes) formulation of the flexible appendage dynamics. In is well known, e.g., see [25], that such formulation can adequately approximate distributed-parameter dynamics both in feedforward and feedback control problems. We take flexible deflection of the appendages along the axis Oy'' to be of the form

$$y(t,\xi) = \begin{cases} \sum_{j=1}^{N_m} q_j(t)\phi_j(\xi - a) & \text{for } \xi \in [a,\ L+a] \\ \sum_{j=1}^{N_m} -q_j(t)\phi_j(-\xi - a) & \text{for } \xi \in [-L-a,\ -a] \end{cases}, \tag{3}$$

where q_j are modal coordinates, N_m is the number of the assumed modes considered, and $\phi_j(\xi)$ are shape functions of the appendage deformation. Following usual practice, we take $\phi_j(\xi)$ to be modal functions of a clamped (free) beam.

By substituting (3) into (1) and computing the integrals, we can present the kinetic energy in the form

$$T = \frac{1}{2}(J + I_1 + J_a\cos^2\psi)\dot{\theta}^2 + \frac{1}{2}(I_2 + J_a)\dot{\psi}^2 + \cos\psi\dot{\theta}m_{\theta q}^T\dot{q} + \frac{1}{2}\dot{q}^T M_{qq}\dot{q}, \tag{4}$$

where the modal cross-inertia vector $m_{\theta q} \in \Re^{N_m}$ and the modal inertia matrix $M_{qq} \in \Re^{N_m, N_m}$ are defined through the shape functions (3) as follows:

$$(m_{\theta q})_j = 2\mu\int_a^{a+L}\xi\phi_j(\xi - a)d\xi \tag{5}$$

$$(M_{qq})_{jk} = 2\mu\int_a^{a+L}\phi_j(\xi - a)\phi_k(\xi - a)d\xi \tag{6}$$

Note that for $\phi_j(\xi)$ being the modal functions of the uniform clamped-free beam, the matrix M_{qq} is diagonal, since these functions are orthogonal to each other in the space $\mathcal{L}_2(0, L)$, e.g., see [25].

By substituting (3) into (2), we obtain the potential energy in the form

$$\Pi = \frac{1}{2} q^T K_{qq} q, \tag{7}$$

where $K_{qq} \in \Re^{N_m, N_m}$ is the modal stiffness matrix. The entries of the matrix K_{qq} are defined as follows:

$$(K_{qq})_{jk} \quad = \quad 2EI \int_a^{a+L} \phi_j''(\xi - a)\phi_k''(\xi - a)d\xi, \tag{8}$$

where prime denotes differentiation with respect to the spatial coordinate ξ. Note that for the modal functions of the uniform clamped-free beam, their second derivatives are orthogonal to each other in the space $\mathcal{L}_2(0, L)$, e.g., see [25]. Hence, for the beam modal functions taken as shape functions, the matrix K_{qq} is diagonal.

Using expressions for the kinetic energy (4) and potential energy (7), we obtain system equations of motion as Lagrange equations of the second kind. These equations are of the form

$$(J_1 + J_a \cos^2\psi)\ddot{\theta} + \cos\psi\, m_{\theta q}^T \ddot{q} - 2\cos\psi \sin\psi\, J_a \dot{\theta}\dot{\psi} - \sin\psi\, \dot{\psi} m_{\theta q}^T \dot{q} = \tau_\theta, \tag{9}$$

$$J_2 \ddot{\psi} + \cos\psi \sin\psi\, J_a \dot{\theta}^2 + \sin\psi\, \dot{\theta} m_{\theta q}^T \dot{q} = \tau_\psi, \tag{10}$$

$$\cos\psi\, m_{\theta q} \ddot{\theta} + M_{qq}\ddot{q} - \sin\psi\, \dot{\theta}\dot{\psi} m_{\theta q} + K_{qq} q = 0, \tag{11}$$

where τ_θ is the base drive torque, τ_ψ is the pitch drive torque, $J_1 = J + I_1$ and $J_2 = I_2 + J_a$.

Parameters of the simulation model are chosen to represent that of some representative telecommunication satellites. In the design of a laboratory testbed, the parameters will be scaled down so that their interrelation provides for motion and control patterns similar to that of the simulations. The parameters used in the simulation study are presented in Table 1.

We found that by taking the shape functions $\phi_j(\xi)$ to be modal functions of a uniform free-clamped beam, it is sufficient to consider only one mode in the simulation. For the numerical integration of the system equations of motion, the integrals (5), (6), and (8) have been computed numerically.

The drive torques τ_θ and τ_ψ in (9), (10) are set by the control system as a sum of the PD feedback and feedforward terms. We assume herein that the back e.m.f. torque in the drives is negligible compared to the derivative feedback term, and the drive torques are as follows

$$\tau_\theta \quad = \quad u_\theta - k_\theta(\theta - \theta_d) - b_\theta(\dot{\theta} - \dot{\theta}_d), \tag{12}$$

$$\tau_\psi \quad = \quad u_\psi - k_\psi(\psi - \psi_d) - b_\psi(\dot{\psi} - \dot{\psi}_d), \tag{13}$$

where k_θ, b_θ, k_ψ, and b_ψ are feedback gains; $\theta_d(t)$ and $\psi_d(t)$ define reference motions for the drive servo-systems; u_θ and u_ψ are feedforward inputs to the drives.

Note that the PD controller (12)–(13) implements a collocated feedback of the actuator positions and velocities and does not use any information on the system flexible dynamics.

To choose feedback gains of the PD controller (12)– (13), the nonlinear system (9)–(13) was linearized in the vicinity of the steady setpoint θ_0, ψ_0. Denoting the coordinate variation vector by $x = [(\theta - \theta_0) \;\; (\psi - \psi_0) \;\; q^T]^T$ and the feedforward control by $u = [u_\theta \; u_\psi]^T$, we obtain the linearized closed-loop system (9)–(13) in the form

$$M(\psi_0)\ddot{x} + B\dot{x} + Kx = Du, \tag{14}$$

where the linearized inertia matrix $M = M(\psi_0)$ depends on the pitch angle setpoint ψ_0.

Expressions for the matrices M, B, K, and D in (14) can be derived from (9)–(11) and are as follows

$$M = \begin{bmatrix} J_1 + J_a\cos^2\psi_0 & 0 & m_{\theta q}^T \cos\psi_0 \\ 0 & J_2 & 0 \\ m_{\theta q}\cos\psi_0 & 0 & M_{qq} \end{bmatrix}, \qquad K = \begin{bmatrix} k_\theta & 0 & 0 \\ 0 & k_\psi & 0 \\ 0 & 0 & K_{qq} \end{bmatrix},$$

$$B = \mathrm{diag}(b_\theta, b_\psi, 0), \qquad D = [1 \;\; 1 \;\; 0], \tag{15}$$

Parameter meaning	Notation	Value
Appendage length	L	30 m
Linear density of appendages	μ	0.2 kg/m
Appendage stiffness	EI	1500 N·m^2
Hub radius	a	1 m
Moments of inertia	I_1, I_2	2000 kg·m^2
Base inertia	J	2000 kg·m^2

Table 1: Parameters of the simulation model

where 0 denotes zero matrices of appropriate dimensions. The linearized system (14), (15) depends on the operating pitch angle ψ_0.

For design simplicity, we choose P and D feedback gains for both drives to be the same, that is

$$k_\theta = k_\psi = k_P, \quad b_\theta = b_\psi = k_D, \tag{16}$$

Quality of the PD controller design can be characterized by a stability margin s of the closed-loop system. The stability margin defines the rate of the transient process decay in the closed-loop system, and it can be defined as $s = -\max_j \mathrm{Re}\,(\lambda_j)$, where λ_j denotes a j-th eigenvalue of the system. A numerically obtained dependence of the stability margin for system (14) on the feedback gains (16) is shown in Figure 3. It has a clearly expressed maximum for certain values of the gains k_P and k_D.

The stability margin, however, depends on the pitch angle ψ_0. Let us express this dependence in the form $s = s(k_P, k_D; \psi_0)$. Since the designed controller should work well for any setpoint ψ_0 within given limits, we consider a *guaranteed* stability margin δ, which is the worst stability margin for all pitch angles and given feedback gains.

$$\delta(k_P, k_D) = \min_{\psi_0} \; s(k_P, k_D; \psi_0)$$

Figure 4 shows a numerically obtained dependence of the guaranteed stability margin δ on the feedback gains k_P and k_D. The approximate values of the gains at the maximum are

$$k_P = 460, \quad k_D = 920 \tag{17}$$

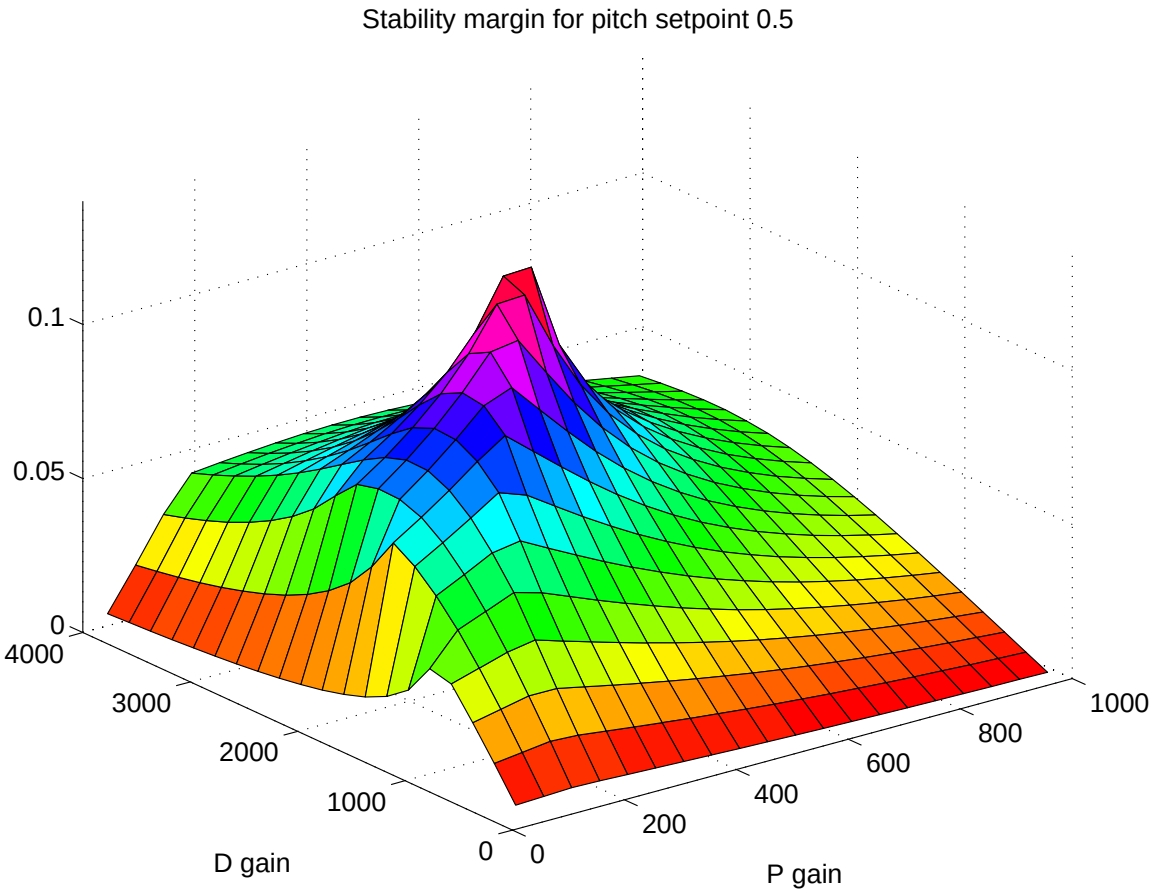

Figure 3: Dependence of the stability margin $s = -\max_j \mathrm{Re}\ \lambda_j(A)$ on the P and D feedback gains k_P and k_D. Pitch angle setpoint is $\psi_0 = 0.5$.

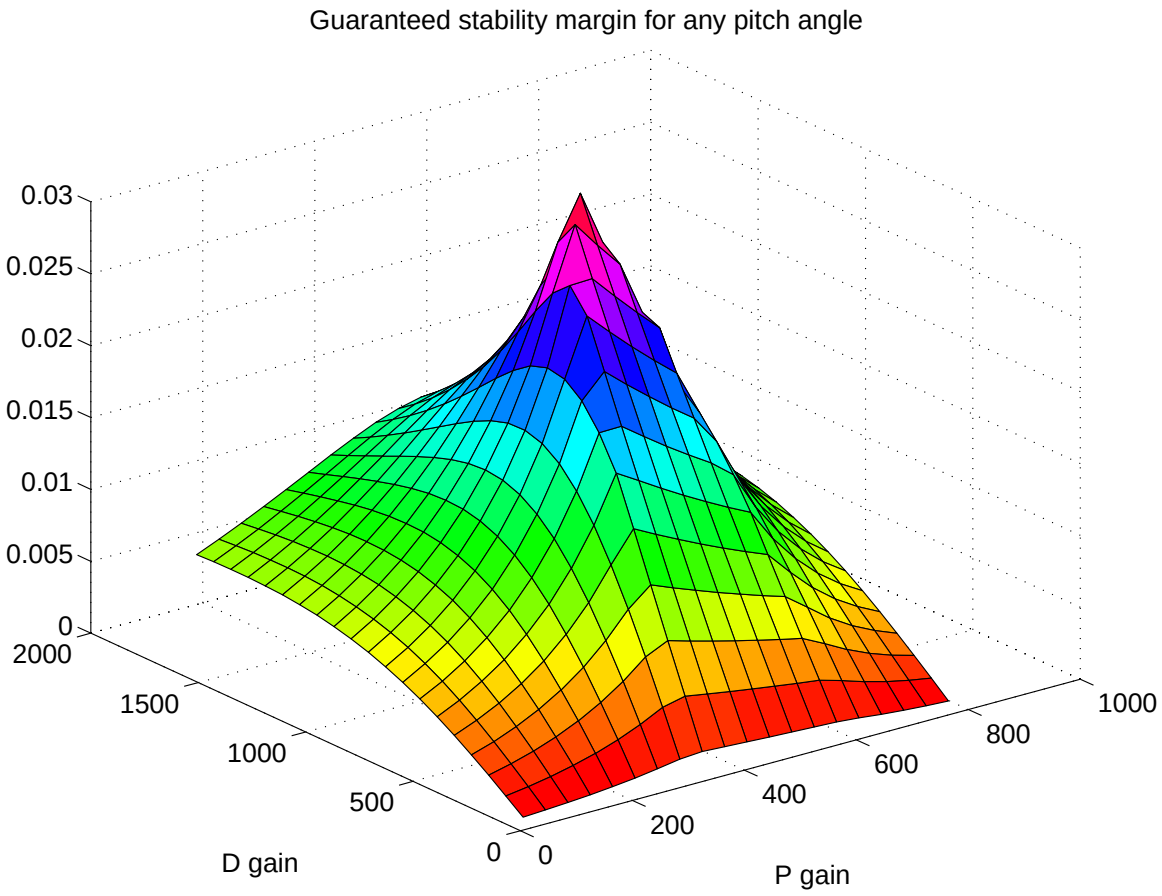

Figure 4: Dependence of the guaranteed stability margin $\delta = \min_{\psi_0} \; s(k_P, k_D; \psi_0)$ on the P and D feedback gains k_P and k_D.

The feedback gains (16), (17) were chosen for the feedback controller (12)–(13) and are used in the subsequent simulations.

Figure 5 shows the results of a full nonlinear simulation for the response of the system (9)–(13) to the step-wise change in the setpoints θ_0 and ψ_0. The PD feedback controller gains in Figure 5 are the guaranteed optimal stability margin gains (16), (17). The response exhibits significant and persistent oscillations of the appendage deformation and control torque. These oscillations are highly undesirable and suggest that an application of a feedforward signal would be instrumental to speed up the system response and make it less oscillatory. Simulations also show that with the change of ψ_0 the oscillation frequencies may vary by as much as 30-40%. Note that further improvement of the system response is only possible with a feedforward controller, since the feedback controller used is already optimized.

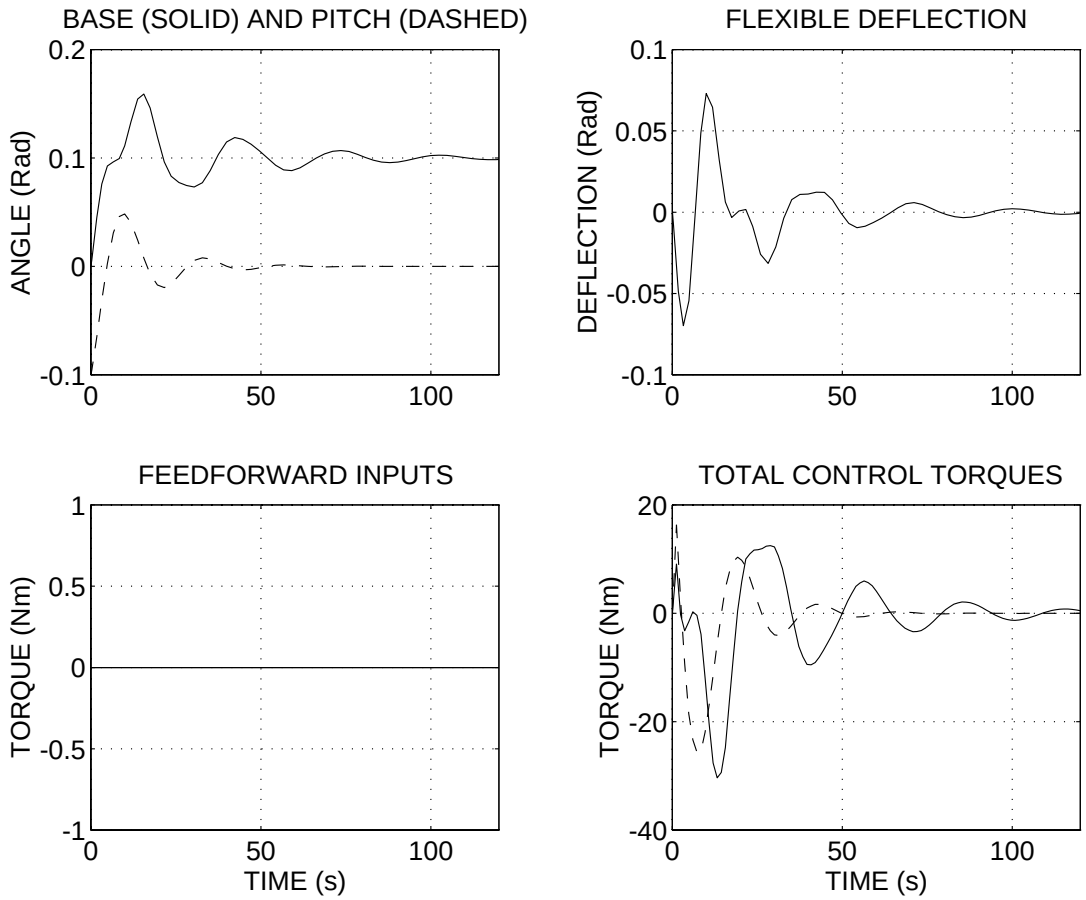

Figure 5: Nonlinear model simulation of the step response for the guaranteed optimal feedback gains: $k_P = 460$, $k_D = 920$. Pitch angle setpoint $\psi_0 = 0$

3 Feedforward shape optimization

This section introduces an optimization problem for computing a feedforward input shape in a rest-to-rest slewing maneuver of the system. A numerical iterative method for the feedforward computation is described. This method converges quickly in the simulation and gives very good control results.

Let us consider a rest-to-rest slewing maneuver of the flexible spacecraft control testbed system shown in Figure 1. At initial time $t = 0$, the system is at rest with attitude angles $\theta(0) = \theta_0$, and $\psi(0) = \psi_0$. The control objective is to slew the system so that the maneuver is completed at the final time $t = T_c$. At the time $t = T_c$, the system should be at rest with desired final attitude angles $\theta(T_c) = \theta_f$, and $\psi(T_c) = \psi_f$.

We plan the reference trajectories $\theta_d(t), \psi_d(t)$ in the PD controller (12)–(13) so that they provide a general desired pattern of motion. We then choose the feedforward control to achieve the desired control objective, which is the absence of vibrations at the end of the maneuver. We compute the reference trajectory to be a straight line in the actuator coordinate space and a third order polynomial in time. This trajectory is fully defined by the initial and the desired final coordinates of the system.

3.1 Parametrization of the control problem

As stated above, the feedforward signals $u_\theta(t)$ and $u_\psi(t)$ in the controller (12)–(13) will be optimized numerically to achieve the optimal performance of the maneuver. To facilitate iterative numerical optimization, we describe the feedforward signals $u_\theta(t)$ and $u_\psi(t)$ as functions of time by using a finite number of parameters. These parameters will define the feedforward sequences and the optimization procedure will optimize these parameters with regard to the control objective.

Let us divide the interval $[0, T]$ into $(n_u + 1)$ subintervals by introducing a sequence of sampling times $\{T_j\}_{j=0}^{n_u+2}$, where $T_0 = 0$, and $T_{n_u+2} = T_c$. We consider feedforward inputs $u_\theta(t)$ and $u_\psi(t)$ which are linear combinations of the first-order B-spline functions $B_j(t)$. Each $B_j(t)$ is a piece-wise linear function, such that $B_j(T_j) = 1$, $B_j(T_{j-1}) = B_j(T_{j+1}) = 0$ and $B_j(t) = 0$ outside the support interval $[T_{j-1}T_{j+1}]$. The feedforward inputs can be written in the form

$$\begin{bmatrix} u_\theta(t) \\ u_\psi(t) \end{bmatrix} = \sum_{j=1}^{n_u} w_j B_j(t), \tag{18}$$

where $w_j = \mathrm{col}(w_{\theta,j}, w_{\psi,j})$ are the weight vectors. The feedforward inputs (18) are piece-wise linear functions with the values $w_{\theta,j}$ and $w_{\psi,j}$ at the interpolation nodes T_j. The shape of the feedforward (18) and of the B-spline functions $B_j(t)$ is illustrated in Figure 6.

It is possible to use B-splines of a different order in the expansion (18). In particular, zero-order B-splines will give a piece-wise constant feedforward (18), while cubic B-splines will result in a twice continuously differentiable feedforward. The paper [19] considers an optimization scheme similar to that used in this paper. A feedforward expansion of the form (18) is used in [19] with trigonometric functions used in the expansion rather than B-splines $B_j(t)$. B-spline expansions of the form (18) are used for feedforward control shaping in the papers [20, 21]. In our simulations, the B-splines provided better estimate of the optimal feedforward profile with less terms than for a trigonometric expansion. Note that the approach to be presented can be, in principle, used with a different parametrization of the control, e.g., with pulse switching times used as parameters in an on-off control.

The feedforward (18) is defined by the weights $w_{\theta,j}$, and $w_{\psi,j}$, which we collect in the *input shape vector*

$$U = [w_{\theta,1} \ \ldots \ w_{\theta,n_u} w_{\psi,1} \ \ldots \ w_{\psi,n_u}]^T \in \Re^{2n_u} \tag{19}$$

The objective of the slewing maneuver control is to achieve the desired final system state at the time T_c - the attitude angles θ and ψ should be those desired, the flexible coordinate q and rates of all coordinates should be zero. We introduce an output vector

$$Y = \left[\theta(T_c) - \theta \ \ \psi(T_c) - \psi \ \ q^T(T_c) \ \ \dot{\theta}(T_c) \ \ \dot{\psi}(T_c) \ \ \dot{q}^T(T_c)\right]^T \in \Re^{4+2N_m} \tag{20}$$

This vector defines the terminal error of the maneuver completion.

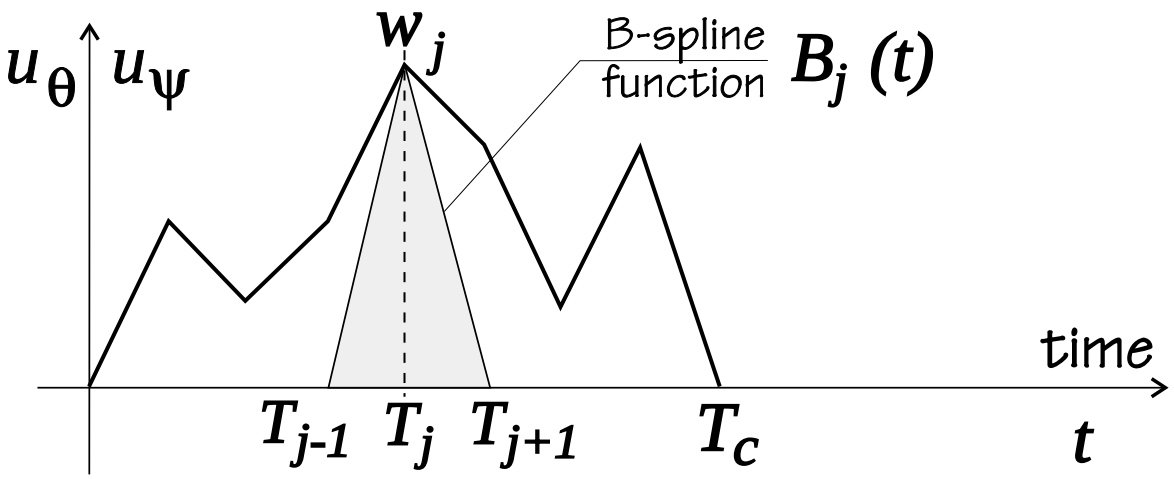

Figure 6: Shape of the feedforward control

3.2 Regularized terminal control problem

For a given maneuver, the input shape vector U (19) defines the output vector Y (20). This dependence can be written in the form

$$Y = S(U, p), \tag{21}$$

where S is a nonlinear mapping, and $p \in \Re^{n_p}$ is a parameter vector defining the maneuver. In this section, we assume the maneuver (and, thus, the vector p) to be fixed, and temporarily ignore the dependence on the second argument in (21). Let us denote the input and output dimensions in (21) in accordance with (19) and (20) as $N_U = 2n_u$, $Y \in \Re^{N_Y}$ and $N_Y = 4 + 2N_m$, $U \in \Re^{N_U}$.

The nonlinear mapping S in (21) is not available to us analytically. However, it can be determined pointwise by applying the feedforward control U (19) in the maneuver simulation and measuring the system output vector Y (20). Under broad conditions on the controlled system, the mapping (21) is smooth (continuously differentiable).

The control objective is to find an optimal feedforward shape vector U that achieves the terminal condition $Y = 0$ with a minimal expenditure of control resources. Following [22], we express this objective through minimization of a single quadratic performance index of the form

$$J = \|Y\|^2 + \rho\|U\|^2 \rightarrow \min , \tag{22}$$

where $\rho > 0$ is a small (regularization) parameter. For $\rho \ll 1$, by minimizing (22), one can cause the terminal error $\|Y\|$ to be as small as needed. It can be proved theoretically, see [22], that for $\rho \rightarrow 0$ the solution U to (21), (22) approaches an optimal quadratic solution to the terminal control problem

$$\|Y\| = 0; \qquad \|U\|^2 \rightarrow \min , \tag{23}$$

It is much easier to numerically solve the nonlinear least square problem (21), (22), than the constraint optimization problem (21), (23). At the same time, by choosing an appropriate $\rho \ll 1$ the solutions to these two problems can be made identical from practical point of view. For the application being considered this can be seen from the simulation results presented below.

Note that in accordance with (18), (19), the quadratic optimality condition $\|U\|^2 \rightarrow \min$ closely represents the fuel optimality condition: $\int_0^T [u_\theta^2(t) + u_\psi^2(t)]dt \rightarrow \min$.

The solution of the nonlinear least square problem (21), (22) can be computed iteratively in a conceptually simple way. For this purpose, we introduce the Jacobian (gradient) matrix for the mapping (21)

$$G = \frac{\partial Y}{\partial U} = \frac{\partial S(U;p)}{\partial U} \in \Re^{N_Y, N_U} \tag{24}$$

The columns of the matrix G define the sensitivity of the sampled system output Y (20) to the variation of the respective components of the vector U in the maneuver defined by the vector p. These columns of G can be determined by means of a secant (finite-difference) estimation, by in turn varying components of the vector U and observing the corresponding variations of the components of the output vector Y.

We apply Newton-Gauss iterative optimization method to compute a solution to the stated problem. According to this method, the update $\Delta U_{\mathbf{k}} = U_{\mathbf{k+1}} - U_{\mathbf{k}}$ of the optimal input guess is computed as a product $D^{-1}\text{grad}_U J$, where $\text{grad}_U J$ is the gradient of the optimized functional (21) and D is a modified Hessian (matrix of the second derivatives) of J [26]. By differentiating (21) with respect to U, we obtain $\text{grad}_U J = \rho U + G^T Y$, where G is the input/output sensitivity matrix (24). The Newton-Gauss method uses the modified Hessian D which is obtained by differentiating the expression for $\text{grad}_U J$ for a second time with respect to U and neglecting the derivatives of G in the result [26]. Thus, the modified Hessian matrix D has the form $D = \rho I + G^T G$.

The Newton-Gauss iterative update of the input vector U that we use for the optimization thus has the form

$$U_{\mathbf{k+1}} = U_{\mathbf{k}} - (\rho I + G^T G)^{-1}(\rho U_{\mathbf{k}} + G^T Y_{\mathbf{k}}), \tag{25}$$

where the bold subscript denotes an iteration number. Each iteration in (25) assumes application of the calculated feedforward input shape (19) defined by the vector $U_{\mathbf{k}}$ to a repetition of the same slewing maneuver defined by the parameter vector p and obtaining the corresponding task output vector (20), $Y_{\mathbf{k}} = S(U_{\mathbf{k}}, p)$. As discussed above, the Jacobian G in (25) can be computed by a secant (finite difference) method, which involves only forward simulations of the system. Thus, once a forward simulation model of a maneuver is available, implementation of the proposed method is straightforward and conceptually simple.

The estimation of the matrix G need not be done at each iteration step. In the simulation results below it was sufficient to compute G only twice, and use the same matrix in three sequential Newton-Gauss update steps each time.

3.3 Optimization results

The feedforward input shape optimization in the rest-to-rest maneuvers of the flexible spacecraft testbed system described in Section 2 was implemented, with the duration of the maneuver taken as $T_c = 25$. As seen from Figure 5, this is close to the lowest eigenfrequency oscillation period of the closed-loop system, which makes this nonlinear control problem very difficult. Making T_c larger simplifies the problem, which becomes less interesting for the simulation study. Shortening T_c significantly results in a sharp increase of the appendage deformations and amplitude of the control effort.

The control sampling times T_j in (18) were chosen to be uniformly distributed in the interval $[0, T_c]$ with an intersampling interval $T_{j+1} - T_J = T_c/10$. Thus, each of the two feedforward inputs u_θ and u_ψ is a linear combination of $n_u = 9$ first-order B-spline functions, and the input shape vector (19) has dimension $N_U = 2n_u = 18$. This input dimension allows us to obtain a reasonable trade-off between achieving the terminal condition, which is imposed on the six components of the system state vector at $t = T_c$, and the quadratic optimality of the feedforward input.

In our implementation of the Newton-Gauss iterative optimization procedure (25), an estimate of the input/output sensitivity matrix G is periodically updated by means of a finite difference (secant) method. The control penalty parameter ρ in (21) is chosen to provide a trade-off between the terminal condition $Y = 0$ and the fuel optimality of the feedforward condition $\|U\|^2 \rightarrow \min$. To achieve this trade-off, we chose the weight ρ according to the regularization approach of [27] to be of the order of the smallest singular value of the matrix $G^T G$. In the numerical experiments, any ρ between $1 \cdot 10^{-8}$ and $2 \cdot 10^{-7}$ worked well. In all subsequent results, $\rho = 4 \cdot 10^{-8}$ was used.

Figure 7 illustrates typical results of the slewing maneuver simulation obtained for the optimized feedforward control shapes. Improvement in the system's transient behavior is evident with the computed optimized feedforward. There are no visible oscillations after $t = T_c = 25$. In fact, for the chosen value of ρ the terminal error is $\|Y\| \approx 10^{-4}$. This is a reasonable accuracy for a numerical method. For a practical implementation of a feedforward control, the terminal error caused by mis-modeling would be much larger than this numerical error. Simulations show that the computed feedforward is reasonably robust to the modeling error, as might be expected from the quadratic optimal (fuel optimal) control.

The closed-loop step response in the absence of feedforward is illustrated in Figure 5 and exhibits visible oscillations lasting till $t = 100$, i.e., four times longer than with the feedforward. At the same time, the maximum applied torque amplitude of Figure 7 is of the same order as that in Figure 5, despite a much larger amplitude of the slewing motion.

The simulation results show that the method developed for the feedforward control computation offers a high-quality solution of the terminal control problem in the slewing maneuver of the flexible satellite.

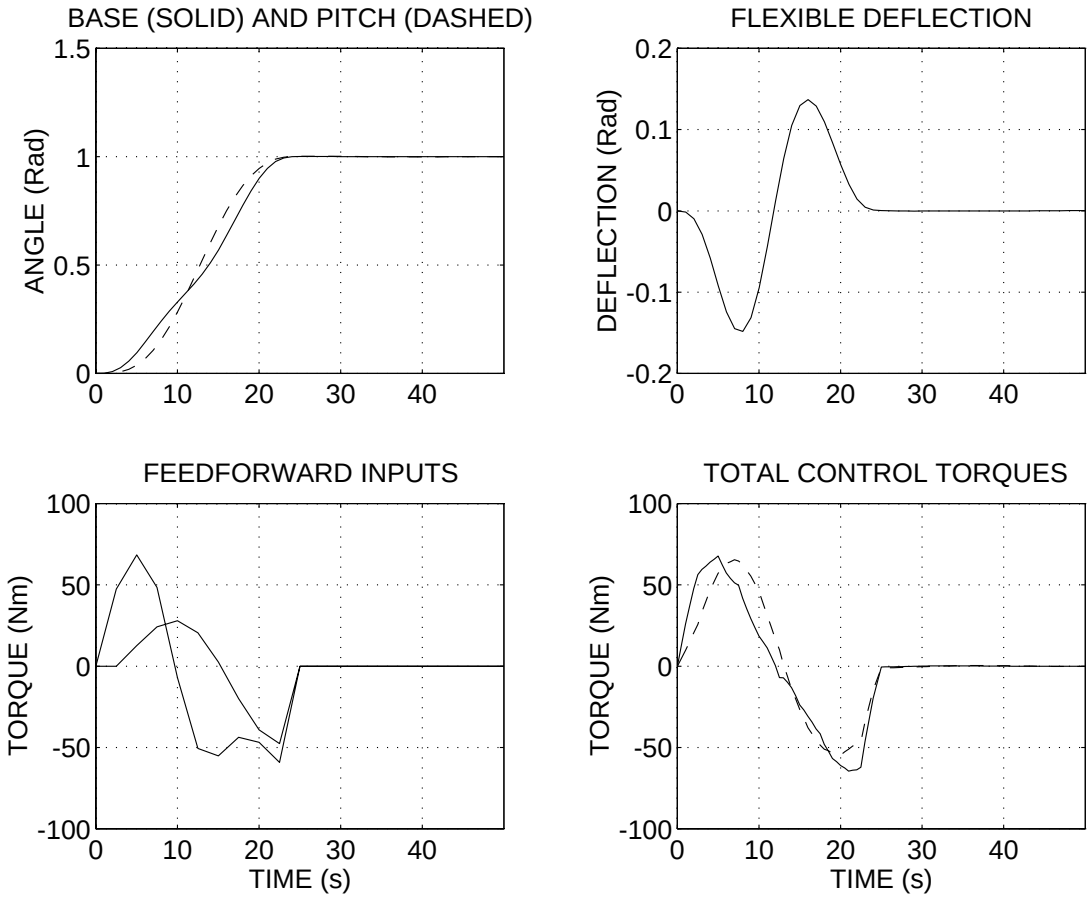

Figure 7: Simulation results for the optimized shape of the feedforward control.

4 Conclusions

This paper presents some potentially useful results for the development of on-board control systems for modern flexible spacecraft.

We described a CSA testbed for control of spatial slewing maneuvers of a flexible spacecraft. The testbed contains electric drives that control attitude angles of a rigid hub with flexible appendages. The testbed system models a satellite with flexible solar arrays and possesses characteristic features of such systems including the nonlinear dynamics of a rigid body rotation.

The paper proposed a technique for optimization-based input shaping control of nonlinear flexible space systems. The technique presented has two important distinct features. First, a regularized quadratic performance index is optimized for a free-end problem, instead of solving a terminal control problem. By choosing the regularization weight to be small, a small terminal error can be obtained. At the same time, it is much easier to compute a solution of the regularized problem than of a boundary-value problem associated with the terminal control. The proposed method is straightforward and easy to implement requiring only a forward simulation model for the maneuver to be available.

The nonlinear input shaping controller designed and validated in this paper computes a feedforward input shape which is optimal with respect to the regularized quadratic performance index. The iterative nonlinear optimization can be computed off-line, before the beginning of the maneuver. A detailed simulation study showed that the suggested approach is capable of very accurate input shaping control.

References

[1] Aspinwall, D.M. "Acceleration Profiles for Minimum Residual Response," *Transactions of ASME. Journal of Dynamical Systems Measurement and Control*, Vol. 102, No. 1, 1980, pp. 3-6.

[2] Gorinevsky, D.M. "Deceleration of an Oscillatory System," *Mechanics of Solids*, Vol. 20, No. 4, 1985, pp. 52–56.

[3] Meckl, P.H. "Robust Motion Control of Flexible Systems Using Feedforward Forcing Functions," *Proceedings of the American Control Conference*, San Francisco, CA, 1993, pp. 2690–2694.

[4] Meckl, P.H., and Seering W.P. "Minimizing Residual Vibrations for Point-to-Point Motion," *Tr. ASME. Journal of Vibration, Acoustics, Stress, and Reliability in Design*, Vol. 107, October 1985, pp. 378–382.

[5] Swigert, C.J. "Shaped Torque Techniques," *AIAA Journal of Guidance, Control, and Dynamics*, Vol. 3, No. 1, 1980, pp. 460–467.

[6] Yamaura, H. and Ono, K. "Vibrationless Starting and Stopping Control for a Flexible Arm," *JSME International Journal Ser. III. Vibration, Control Engineering, Engineering for Industry* Vol. 32, No. 3, 1989, pp. 413–420.

[7] Singer, N.C., and Seering, W.P. "Preshaping Inputs to Reduce System Vibration," *Transactions of ASME. Journal of Dynamical Systems Measurement and Control*, Vol. 112, No. 1, 1990, pp. 76–82.

[8] Singhose, W., Derezinski, S., and Singer, N. "Extra-Insensitive Shapers for Controlling Flexible Spacecraft," *Proceedings of AIAA Guidance, Navigation, and Control Conference*, Scottsdale, AZ, 1994.

[9] Tzes, A., and Yurkovich, S. "An Adaptive Input Shaping Control Scheme for Vibration Suppression in Slewing Flexible Structures," *IEEE Transactions on Control Systems Technology*, Vol. 1, No. 2, 1993, pp. 114–121.

[10] Watkins, J., and Yurkovich, S. "Input Shaping Controllers for Slewing Flexible Structures," *Proceedings of the First IEEE Conference on Control Applications*, Dayton, OH, 1992, pp. 188–193.

[11] Bayo, E. "A Finite Element Approach to Control the End-Point Motion of a Single Flexible-Link Robot," *Journal of Robotic Systems*, Vol. 4, 1987, pp. 63–75.

[12] Bayo, E., Serna, M.A., Papadopulos, P., and Stube, J. "Inverse Dynamics and Kinematics of Multi-Link Elastic Robots. An Iterative Frequency Domain Approach," *International Journal of Robotics Research*, Vol. 8, No. 6, 1989, pp. 49-92.

[13] Khorrami, F., Jain, S., and Tzes, A. "Experiments on Rigid Body-Based Controllers with Input Preshaping for Two-Link Flexible Manipulator," *IEEE Transactions on Robotics and Automation*, Vol. 10, No. 1, 1994, pp. 55–65.

[14] Singh, T., and Vadali, S.R. "Input-Shaped Control of Three-Dimensional Maneuvers of Flexible Spacecraft," *AIAA Journal of Guidance, Control, and Dynamics*, Vol. 16, No. 6, 1993, pp. 1061–1068.

[15] Pfeiffer, F. "A Feedforward Decoupling Concept for the Control of Elastic Robots," *Journal of Robotic Systems*, Vol. 6, 1989, pp. 407–416.

[16] Pfeiffer, F., and Gebler, B. "A Multistage Approach to the Dynamics and Control of Elastic Robots," *Proceedings of IEEE Int. Conference on Robotics and Automation*, Philadelphia, PA, 1988, pp.2–8.

[17] Pfeiffer, F., Gebler, B., and Kleeman, U. "On Dynamics and Control of Elastic Robots," *Proceedings of SYROCO'88*, Karlsruhe, Germany. Pergamon Press, Oxford, 1989, pp. 41–45.

[18] Meyer, J.L., Silverberg, L. "Fuel optimal propulsive maneuver of an experimental structure exhibiting spacelike dynamics," *AIAA Journal of Guidance, Control, and Dynamics*, Vol. 19, No. 1, 1996, pp. 141–149.

[19] Cheng, W., Wen, J.T., and Hughes, D. "Experimental Results of Learning Controller Applied to Tip Tracking of a Flexible Beam," *Proceedings of American Control Conference*, San Francisco, 1993, pp. 987–991.

[20] Gorinevsky, D.M. "Experiments in Direct Learning of Feedforward Control for Manipulator Path Tracking," *Robotersysteme*, Vol. 8, 1992, pp. 139–147.

[21] Gorinevsky, D., Torfs, D., and Goldenberg, A.A. "Learning Approximation of Feedforward Dependence on the Task Parameters: Experiments in Direct-Drive Manipulator Tracking," *Proceedings of American Control Conference*, Seattle, June 1995.

[22] Gorinevsky, D.M. "On the Approximate Inversion of Linear System and Quadratic-Optimal Control". *Journal of Computational and System Science International*, Vol. 30, No. 6, 1992, pp. 6–23.

[23] Dohrmann, C.R., and Robinett, R.R. "Input Shaping for Three-Dimensional Slew Maneuvers of Flexible Spacecraft," *Proceedings of American Control Conference*, Baltimore, June 1994, pp. 2543–2547.

[24] Wie, B. et al. "Robust Fuel- and Time-optimal Control of Uncertain Flexible Space Structures," *Proceedings of American Control Conference*, San Francisco, CA, June 1993, pp. 2475–2479.

[25] Gorinevsky, D.M. "Galerkin Method in Control of Distributed Flexible Systems", *Computer Methods in Applied Mechanics and Engineering*, Vol. 109, 1993, pp. 107-128.

[26] Dennis, J.E., and Schnabel, R.B. *Numerical Methods for Unconstrained Optimization and Nonlinear Equations*, Prentice Hall, Englewood Cliffs, 1983.

[27] Tikhonov, A.N., and Arsenin, V.Ya. *Solutions of Ill-Posed Problems*. Halsted Press, Washington, 1977.